Impact of human CD8+ T cell senescence on ^{89}Zr radiolabelling and PET imaging

Jonas Bystrom[1], Amaia Carrascal-Miniño[2], George P Keeling[2], Truc Pham[2], Conor Garrod-Ketchley[1], Johannes Schroth[1], Rafael T. M. De Rosales[2], Samantha YA Terry[2], Sian M. Henson[1]

1. Centre for Translational Medicine and Therapeutics, William Harvey Research Institute, Queen Mary University of London, London, EC1M 6BQ, UK
2. School of Biomedical Engineering & Imaging Sciences, King's College London, St Thomas' Hospital, London, SE1 7EH, UK

Correspondence: Jonas Bystrom or Sian M. Henson
William Harvey Research Institute, Queen Mary University of London, London, EC1M 6BQ, UK
Tel: +44 (0)20 7882 2100
E-mail: j.bystrom@qmul.ac.uk or s.henson@qmul.ac.uk

Abstract

The ability of CD8+ T cells to protect against infection and malignant transformation diminishes with age. Novel means to assess cells' functional deficits *in vivo* are being made available such as total-body positron emission tomography (PET) and radiotracers with long half-lives. We show here that human CD8+ T cells isolated from young and old individuals can be labelled using zirconium-89 (^{89}Zr) and their functionality assessed *in vivo*.

Methods

Fresh and cryopreserved CD8+ T cells from young and old individuals were labelled with varying activities of [^{89}Zr]Zr-oxine. CD8+ T cells were assessed for DNA damage and survival, subsequent to *in vitro* culture in the presence or absence of antioxidants. ^{89}Zr-labelled CD8+ T cells were injected intravenously in NSG mice and whole body cell migration assessed using PET imaging.

Results

Fresh and cryopreserved CD8+ T cells from young and old individuals showed no difference in ^{89}Zr-labelling, radionuclide retention or CD8+ T cell distribution. ^{89}Zr induced partial cell death and DNA damage, which was no longer visible after four days. The level of DNA repair observed in old samples was highly variable. Labelled CD8+ T cells whole body biodistribution in healthy mice was followed longitudinally using PET imaging. ^{89}Zr efflux from cells, seen *in vitro*, did not occur *in vivo*. Longitudinal PET imaging indicated different homing preferences between CD8+ T cells from young and old individuals.

Conclusion

We have established a strategy to label and track the biodistribution of cryopreserved CD8+T cells. Further study is required to understand differences in migratory behaviour in CD8+ T cells isolated from old and young individuals.

Introduction

Positron emission tomography (PET) imaging allows for non-invasive total body imaging with a 10 - 40 fold increase in sensitivity compared to conventional systems (1). Novel pixelated lutetium oxyorthosilicate detectors and improved timing resolution now provide a spatial resolution of 3.5 - 5 mm (1, 2). Such modality enhancements provide the means to analyse immune cell localization in detail, using small numbers of radionuclide-labelled cells (3, 4). Using radionuclides with a long half-life for PET imaging makes the detection of discrete cell populations within defined tissue locations possible (5).

PET radionuclides with a long half-life, such as ^{89}Zr ($t_{1/2}$ = 78.4 hr), can be used for both preclinical and clinical imaging and enable the detection of cells longitudinally from repeat PET scans. ^{89}Zr-labelling can be achieved either indirectly or directly. ^{89}Zr-labelled antibodies have been used to demonstrate the role of CD8+ T cells in tumour immunity and their response to therapy (4, 6). Direct labelling of immune cells provides increased sensitivity and specificity (7, 8) and is achieved through the chelation of ^{89}Zr with four oxine (8-hydroxyquinoline) molecules to generate a metastable complex that can cross cell membranes. This complex dissociates inside cells, depositing ^{89}Zr bound to intracellular proteins (7, 8). A caveat with direct labelling is that lymphocytes are prone to radiation damage, senescence, and cell death (9, 10). However, CAR T cells labelled with ^{89}Zr showed no reduction in cytokine production, migration, tumour cytotoxicity, or *in vivo* antitumor activity when subjected to 70 kBq/10^6 cells (11).

CD8+ T cells can be subdivided into different populations varying in their functional and homing preferences (12). Central memory (CM) CD8+ T cells were shown to provide longer-lasting protective immunity than the effector memory (EM) subset (13). Older individuals, who are more susceptible to malignancies, have an increased proportion of the EM CD45RA re-expressing (EMRA) CD8+ T cells which display reduced proliferative capacity, higher levels of DNA damage and an altered migratory potential (14). It remains unexplored whether this EMRA subpopulation responds differently to cell labelling and whether homing abilities are altered. Additionally, further characterization of these EMRA T cells will be essential if ^{89}Zr is to be used clinically, specifically, whether cryopreservation influences CD8+ T cell phenotype, together with their ability to be labelled and retain ^{89}Zr. This is important as most chronic diseases requiring analysis by PET generally occur at an older age (6). Therefore, it is of interest to determine whether the build-up of EMRA T cells with age influences the ability of ^{89}Zr labelling for imaging.

We show in this study that cryopreservation does not influence the ability of CD8+ T cells isolated from young and old individuals to be labelled with ^{89}Zr. Cryopreserved ^{89}Zr-CD8+ T cells were readily detected using PET imaging and tracked for three days in mice. However, ^{89}Zr retention in CD8+ T cells from old individuals was lower than cells taken from young people. All CD8+ T cells experienced initial DNA damage which was repaired during *in vitro* culture. However, with DNA damage remaining high in CD8+ T cells from old individuals. Labelling of CD8+ T cells and longitudinal assessment by *in vivo* PET scanning indicated retention of ^{89}Zr but different migratory patterns when using young and old T cells. This study suggests that the age of CD8+ T cells should be taken in account during longitudinal PET studies as it may influence the DNA-damage response to ^{89}Zr, and thereby the migratory capacity of the studied cells.

Materials and Methods

Reagents, animals, and cells

^{89}Zr (oxalate) was purchased from Perkin Elmer. Ficol Paque was purchased from GE Healthcare. PBS, RPMI and ascorbic acid and 2-mercaptoethanol (2-ME) was purchased from Merck Millipore. IL-2 and anti-CD3 (OKT3) was purchased from BioLegend. Anti-CD8 magnetic beads were purchased from Miltenyi. Female Nod *scid* gamma (NSG, NOD.Cg-*Prkdc* ^{scid} *IL2rg*^{tm1Wjl}/SzJ) mice aged 6 weeks were purchased from Charles River (UK).

Ethical Approval

Our clinical protocol was approved by the West London & GTAC Research Ethics Committee (20/PR/0921) and all subjects provided written informed consent. We recruited healthy volunteers in two age ranges, young: 23-58 years of age (n = 8), and old: 69-82 years of age (n = 4). Animal experiments were approved by the UK Home Office under The Animals (Scientific Procedures) Act (1986), PPL reference 7008879 (Protocol 6), with local approval from King's College London Animal Welfare and Ethics Review Body.

Cell isolation

Blood (30-60 mL) was obtained from heathy young or old individuals. Peripheral blood mononucleated cells (PBMCs) were isolated using Ficoll Paque. Cells were resuspended in FBS with 10% DMSO and stored in liquid nitrogen or used directly. Cryopreserved PBMCs were thawed, washed once using RPMI, resuspended in RPMI culture medium and stored at 37°C 1 hr prior to the labelling procedure. Cell number was determined using a haemocytometer prior to cell labelling. CD8+ T cells were isolated from PBMCs using Miltenyi magnetic beads and magnetic column as has been described before (15). CD8+ T cells from cryopreserved samples were isolated upon thawing and then treated as the cryopreserved PBMCs prior to labelling.

PET tracer synthesis and cell labelling

^{89}Zr was chelated with oxine forming [^{89}Zr]Zr(oxinate)$_4$ as previously described (7). White blood cells (PBMC or separated CD8+ T cells) were washed with PBS (Ca^{2+}/Mg^{2+} free), resuspended in PBS and mixed with [^{89}Zr]Zr(oxinate)$_4$ with a volume ratio not lower than 30:1 (cells: [^{89}Zr]Zr(oxinate)$_4$), using 3-20x10^6 cells and 5-100 mBq/cell in various experiments. In some experiments, PBMCs were resuspended in PBS containing 0.1 or 10 mg/mL ascorbic acid or 50 µM 2-mercaptoethanol. The labelling reaction was stored at 37°C or 4°C for 30 min, with agitation every 5 min. Subsequent to the labelling reaction, the cells were washed using 50 mL PBS and quantified using a haemocytometer. Labelling efficiency was determined using

a dose calibrator (Capintec) or a 1282 Compugamma CS universal gamma counter (LKB Wallac).

Cell culture

For radiotracer retention and cell proliferation studies, radiolabelled (or vehicle-treated) PBMC or CD8+ T cells were cultured using RPMI, supplemented with 10% FBS, L-Glutamine (2 mM), penicillin and streptomycin (Sigma) and 1 ng/mL IL-2 (Miltenyi). For CD8+ T cell cultures, tissue culture plates were precoated with 0.5 µg/mL anti-CD3 prior to addition of the cells. Cells remaining in the cell cultures were determined at 24hr and 96hr using a haemocytometer and trypan blue to exclude dead cell. Exact number of CD8+ T cells and subpopulations with and without γH2AX was determined by relating proportions determined by FACS: number of PBMCs in culture to the initial number of PBMCs after the cell labelling reaction. Cell-associated radioactivity was measured using a gamma-counter and FACS was used to determine CD8+ T cell phenotype and DNA damage. Based on activity in the cells, determined by the gamma-counter, % of initial activity (%IA) was calculated using a ^{89}Zr standard curve.

Flow cytometry analysis

Flow cytometric analysis was performed using the following antibodies: anti-CD8 PerCP (SK1), anti-CD45RA APC (HI1000), anti-CCR7 PECy7 (G043H7), and CD27 FITC (O323) from BioLegend. γH2AX (BioLegend) was used for intracellular staining with FOXP3 staining buffer (BioLegend). Annexin V FITC was used with binding buffer from BioLegend. All samples were analysed using a FACS Melody (BD Biosciences) and the resulting data examined using FlowJo software (BD Bioscience).

***In vivo* PET imaging of CD8+ T cells**

^{89}Zr-labeled CD8+ T cells (3x10^{6} cells/animal in 100 µL PBS, 36.9 ± 42.8 kBq, single CD8+ T donor per experiment) were anaesthetised (1.5-2.5% isoflurane in oxygen) and injected intravenously at t = 0 hr. Three hours post-injection the mice were re-anaesthetised and placed in a preclinical nanoPET/CT scanner (Mediso); where anaesthesia was maintained, and the bed was heated to maintain a normal body temperature. Two hours of PET acquisition (1:5 coincidence mode; 5 ns coincidence time window) were followed by CT. PET-CT was repeated at t = 24 and 72 hr (2 and 3 hr, respectively). Dynamic PET/CT images were reconstructed using a Monte Carlo-based full-3D iterative algorithm (Tera-Tomo, 400-600 keV energy window, 1-3 coincidence mode, 4 iterations and subsets) at a voxel size of (0.4 × 0.4 × 0.4) mm^{3} and corrected for attenuation, scatter, and decay. Images were co-registered and analysed using VivoQuant v.3.0 (InVicro LLC.) capturing maximum intensity projection (MIP) and transverse plane images. If required, background, not associated with anatomy, were

manually removed. Regions of interest (ROIs) were drawn covering lung, liver and spleen structures based on CT image data and activity accumulation determined. Data is presented as %IA/g.

Statistical analysis

Statistical analysis was performed using GraphPad Prism version 9.5. A Mann-Whitney U test was used to compare differences between groups and Wilcoxon signed rank test within groups, as data was not normally distributed. Data was expressed as mean ± SD and statistically significant differences represented using the following notation: * = $p < 0.05$, ** = $p < 0.01$, *** = $p < 0.005$ and **** = $p < 0.001$.

Results

Total body PET imaging for tracking immune cells holds great promise as a future diagnostic and treatment response modality. Here we focused on optimising the labelling of CD8+ T cells as detailed information of their localization preference *in vivo* might improve our understanding of their role in malignancies and other diseases (6, 16). In particular, we investigated the effect of cryopreservation, as it would be advantageous to isolate cells for [^{89}Zr]Zr-(oxinate)$_4$ labelling and infusion in advance of any PET imaging. Furthermore, as many chronic diseases occur later in life, it is of interest to determine whether old age also negatively influenced the cell labelling process.

We used freshly isolated and cryopreserved PBMCs and CD8+ T cells from volunteers (39.3 ± 14.5 years of age) and old volunteers (77.3 ± 4.5 years of age) for [^{89}Zr]Zr(oxinate)$_4$ cell labelling. A previously established kit-formulation was first used to create [^{89}Zr]Zr(oxinate)$_4$ with a radiochemical yield of 82.3 ± 7.7 %. Figure 1A, shows a representative radio-TLC trace of the successful radiolabelling; this was similar to previous reports (7). PBMC cell number was then determined, indicating a more than 50% loss of cells during the 30 minute labelling process but with no difference between young and old PBMCs (Figure 1B). Activities ranging from 5 to 100 mBq/cell, resulted in a cell labelling efficiency of 63.3 ± 30.5%. Neither cryopreservation nor age influenced cell labelling efficiency (Figure 1C).

To determine whether cryopreservation influenced the ability of cells to retain ^{89}Zr PBMCs were kept in culture and the activity in cells and medium was assessed at one and four days after cell labeling. Freshly isolated PBMCs retained 34.4 ± 15.5% of the initial activity while cryopreserved cells retained 19.5 ± 4.6% after one day of culture ($p = 0.0503$, Figure 1D). Cryopreserved PBMCs from younger volunteers however retained significantly more ^{89}Zr than cells isolated from older participants (4.5 ± 1.8%, $p = 0.0044$). Both freshly isolated and cryopreserved PBMCs released an increasing amount of ^{89}Zr over time (Figure 1D). Comparison of the amount of ^{89}Zr retained inside cells to that released in the supernatant (Figure 1E) yielded similar results as the %IA (Figure 1D). Overall, the data shows no age-related effect on the ability of ^{89}Zr to label immune cells. However, PBMCs from older volunteers retained less radionuclide during *in vitro* culture.

We then assessed how labelling cells with ^{89}Zr influenced their survival and DNA damage response, together with cryopreservation of PBMCs taken from young and old individuals. Cell numbers of freshly isolated and cryopreserved PBMCs with or without ^{89}Zr labelling were enumerated at day one and four of culture (Figure 2A). Cryopreservation affected cells from young or old individuals equally, in that there was a sharp decline in the number of CD8+ T

cells between d0 and d1, cell numbers then remained stable for the duration of culture (Figure 2A). Among PBMCs, CD8+ T cell numbers were not specifically affected at day one and four of culture. However, a trend towards a decline in labelled CD8+ T cell numbers was observed (Figure 2B). This was explored further using Annexin V to determine the amount of cell death following labelling. The addition of ^{89}Zr resulted in a significantly higher proportion of CD8+ Annexin V+ T cells than untreated cells, with the amount of apoptotic CD8+ T cells increasing further after 4 days in culture (Figure 2C). The number of CD8+ T cells from old individuals was lower than that of young but was not altered during culture (Figure 2B). This loss of CD8+ T cells with age has been reported before and is likely not related to the radiolabelling itself (17).

To determine whether intracellular ^{89}Zr altered the DNA damage response in CD8+ T cells from young and old individuals, an assessment of the double strand break associated histone γH2AX was made (Figure 2D). Untreated CD8+ T cells from old individuals tended to have more *ex vivo* DNA damage than young individuals (Figure 2E). After one day of culture the presence of the ^{89}Zr label was found to induce high levels of DNA damage to both young (71.6 ± 24.1% γH2AX+) and old (45.2 ± 12.5% γH2AX+) CD8+ T cells, with a trend for more damage being generated in the CD8+ T cells from young people (Figure 2E). At day four the proportion of young γH2AX+ CD8+ T cells had returned to baseline. However, for old labelled CD8+ T cells the γH2AX-level remained high ($p = 0.018$, Figure 2E). Assessment of number of young CD8+ T cells in cell culture confirmed that γH2AX+ increased at day one but returned to a pre-label level by day 4 ($p = 0.016$, Figure 2F). As the CD8+ T cells from old individuals were less abundant following the labelling procedure when enumerated they failed to show the same increase in DNA damage as young cells. However, their number did not decline and failed to repair but persisted in culture ($p = 0.024$, Figure 2F).

CD8+ T cells are heterogenous and can be subdivided into 4 populations using the cell surface markers CD45RA and CCR7, thereby identifying CD45RA+CCR7+ Naïve, CD45RA-CCR7+ central memory (CM), CD45RA-CCR7- effector memory (EM) and CD45RA+CCR7- EMRA T cells. The EMRA population displays senescent-like characteristics and are expanded in old individuals (14). We assessed whether CD8+ T cell subset composition differed following ^{89}Zr-labelling (Figure 3A). Although the EMRAs were more numerous in older individuals (Figure 3A) the relative subset distribution was not affected by ^{89}Zr-labelling (Figure 3B-E). Additional confirmation that ^{89}Zr-labelling did not drive CD8+ T cell differentiation was also noted when T cells were quantified (Figure 3F-I).

We then assessed whether ^{89}Zr-induced γH2AX+ was overrepresented in any the CD45RA/CCR7 defined CD8+ T cell subsets. While γH2AX+ was found in all four subsets in both young and old individuals the pattern of DNA damage differed. In young cells, γH2AX was high post-labelling but then declined by 4 days, and old cells showed an increase in double strand breaks, which then remained high throughout culture (Figure 4A-D); this could be attributed to the naïve CD8 T cell population (Figure 4A). Total number of CD8+γH2AX+ T cells was unaffected in old cells (Figure E-F). In conclusion, the DNA damage response to ^{89}Zr in old populations is blunted compared to CD8+ T cells taken from young individuals.

As ^{89}Zr labelling leads to enhanced DNA damage and death in CD8+ T cells (Figure 2A-E), we then tested ways to prevent this radiation-induced damage. Inhibition of reactive oxygen species has been used previously to prevent damage (18), as has lowering the temperature during the labelling reaction (7). Therefore, 0.1 and 10 mg/mL ascorbic acid and 50 µM 2-mercaptoethanol was included during the [^{89}Zr]Zr(oxinate)$_4$ labelling reaction. The labelling reaction was also carried out at 4°C. Labelled CD8+ T cells were subsequently kept in culture for analysis of Annexin V binding and expression of γH2AX. The high dose of ascorbic acid (10 mg/mL) and 4°C were found to inhibit the initial [^{89}Zr]Zr(oxinate)$_4$ uptake (Figure 5A). None of the treatments improved ^{89}Zr retention compared to the original conditions performed at 37°C (Figure 5B). Likewise, annexin V and γH2AX expression showed that these strategies were unable to prevent the radiation-induced damage reduced to CD8+ T cells (Figure 5C, D). The phenotype of the CD8+ T cells was also assessed with no evidence of changes in the distribution of the 4 subsets in response to any of the radiation damage-prevention methods used (data not shown). In conclusion this data suggested that conventional treatments to scavenge free radicals do not work on CD8+ T cells.

We have shown that ^{89}Zr causes CD8+ T cell death and DNA damage *in vitro*. To determine whether cryopreservation and age would influence PET imaging studies, 3×10^6 CD8+ T cells from young and old individuals were labelled with [^{89}Zr]Zr-(oxinate)$_4$ and infused into NOD scid gamma (NSG) mice at a final activity of 67.2 kBq and 6.69 kBq for young and old respectively. The CD8+ T cells were tracked using preclinical PET at time points, 3, 24 and 72 hr (Figure 6A-F) and localization defined in terms of percent of initial activity (%IA/g, Figure 6G-K). CD8+ T cells, initially were found localized to lung and liver (3 hr, Figure 6A, D). While young and old CD8+ T cells gradually accumulated in the spleen, a high proportion of old CD8+ T cells remained in the liver (Figure 6G, H) and lung (Figure 6I). During the observation time, old CD8+T cells did accumulate in the spleen at a slower rate compared to young T cells (Figure 6G). Overall, our data indicate that age-related changes to CD8+ T cells result in alterations to the subset balance which may influence localization to specific organs.

Discussion

In this study we have gained important insights that will help to better track immune cell subpopulations using the total-body PET modality. Cryopreserved CD8+ T cells, stored in liquid nitrogen, can be labelled with similar efficiency to freshly isolated cells. Cryopreserved ^{89}Zr-labelled CD8+ T cells were readily detected using PET imaging and tracked for three days post-infusion. In response to labelling, CD8+ T cells experienced initial DNA damage which was associated with cell death. Furthermore, while a significant proportion of the CD8+ T cells from young individuals underwent DNA repair this was not the case when labelling aged cells. Tissue distribution of CD8+ T cells from young and old individuals suggested that there was an age-dependent difference in organ homing with an alteration in migration dynamics between young and old CD8+ T cells. Hence the old CD8+ T cells remained to a larger extent in the liver, while young cells more efficiently infiltrated the spleen of the mice. Although our *in vitro* studies indicate that CD8+ T cells from old individuals do not retain ^{89}Zr as well as the cells isolated from young individuals, the *in vivo* experiments suggest protection *in situ*.

The advent of total body PET with the ability to detect cells with a high sensitivity provides the opportunity to study specific cell subsets that have different homing preferences (2, 16). The high specificity of directly labelled cells have an advantage in that sense, compared to radiolabelled antibodies that can be associated with background (8, 16). In our study, we assessed whether ^{89}Zr labelling influenced CD45RA/CCR7 defined CD8+ T cell subsets differently. Although γH2AX was dramatically upregulated in half to more than two thirds of all the cells, the different subset-proportions were likely not altered by the labelling. We also assessed the influence of ^{89}Zr labelling on aged CD8+ T cells. This is important as old individuals are more likely than young to undergo PET scan assessment for tracking of immune cells (6). Old individuals have proportionally more EMRAs than young (Figure 3A), which has been well reported previously (17, 19). EMRA T cells display hallmarks of senescence in that they express high levels of KLRG1, dysfunctional mitochondria, increased ROS production leading to more DNA damage and a reduced proliferative capacity (15). The DNA damage response (DDR) to ^{89}Zr dose-exposure differed between CD8+ T cells isolated from young and old individuals. Aged naïve T cells had more DNA damage at baseline and went on to upregulate more γH2AX in response to ^{89}Zr, which remained present in the cells at day four of culture suggesting an inefficient DNA repair process. However, it has been documented that naïve CD8+ T cells from old individuals are not truly naïve, some originating from the EMRA subset, potentially explaining our observations (20, 21). There are two pathways to repair DNA double strand breaks (DSB), non-homologous end joining (NHEJ) and homologous recombination (22). Three proteins from the phosphatidylinositol 3-kinase

related kinase family are activated by DSBs, ataxia telangiectasia mutated kinase (ATM), ATM-related kinase, and DNA-dependent protein kinase. Early in the DDR, the phosphorylation of histone H2AX (γH2AX) signals the presence of DSB to repair proteins, which in turn aggregate in ionising radiation-induced foci. The DDR is induced by ROS and possibly by unprotected DNA during telomere attrition in EMRAs (15, 23). The EMRA did not upregulate γH2AX and could therefore be more prone to cell death. Unfortunately, our attempts to prevent radiation-induced DNA damage, both using the ROS scavenger ascorbic acids and by undertaking labelling at low temperature, were unsuccessful. Our *in vitro* studies suggest that the different *in vivo* migratory preference observed between young and old T cells, may only partly be due to radiation induced changes to CD8+ T cell subsets. DNA damage not only kills older EMRA T cells but could contribute to the localization preference shown here. Indeed, ATM activation has been shown to regulate IL-8 to sustain cell migration (24). Furthermore, the chemokine receptor CXCR2 was found to be upregulated in response to p53 (25). Given that we have shown CXCR2 to be upregulated on CD8+ EMRA T cells from people with type 2 diabetes (26), a condition that induces premature immune senescence, it is not unreasonable to speculate that DNA damage could influence the migratory capability of T cells. Interestingly, in cancer patients, the variability to radiation-induced DDR is different in the CD8+ T cell subsets and has been associated with treatment response. For example, a study of advanced or recurrent hypermutated or microsatellite instability-high, mismatch repair deficient uterine cancer patients showed subset differences in their DDR following check-point blockade, with the EMRA subset showing the highest expression of γH2AX in response to irradiation (27). Furthermore, following checkpoint blockade activation of the ATM downstream of γH2AX was only seen in therapeutic responders. It is likely that such a varied response seen when comparing young and old T cells, in our study, would make specific cell populations more prone to radiation-induced death, but potentially altered cellular function that might influence their homing preferences.

Conclusion

Cryopreservation did not affect the ^{89}Zr labelling potential of CD8+ T cells. However, the DDR following labelling was altered in CD8+ T cells isolated from old individuals. Analysis of tissue distribution using ^{89}Zr labelled CD8+ T cells from young and old suggest that there is a difference in migration preference. These findings will have implications to human CD8+ T cell tracking and detailed localization preference using total body PET in response to immune-regulating treatments.

Acknowledgements

We would like to thank Jana Kim and Hannah Greenwood for their help with i.v. injections. This research was supported by Diabetes UK 19/0006057, Barts and the London Charity MGU0536, Royal College of Anaesthetists WRO-2018-0065. Additionally, this work was funded in part by the EPSRC programme for next generation molecular imaging and therapy with radionuclides [EP/S032789/1], the Wellcome/EPSRC Centre for Medical Engineering at King's College London [WT 203148/Z/16/Z], a Wellcome Trust Multiuser Equipment Grant: A multiuser radioanalytical facility for molecular imaging and radionuclide therapy research [212885/Z/18/Z], Research England Confidence in Collaboration scheme, and the MRC Confidence in Concepts scheme. The nanoPET/CT scanner at KCL was funded by an equipment grant from the Wellcome Trust WT 084052/Z/07/Z. For the purpose of open access, the author has applied a CC BY public copyright licence to any Author Accepted Manuscript version arising from this submission. Finally, we thank the research participants for their commitment to this study and their generous donation of blood samples.

Conflict of interest

All authors declare that the research was conducted in the absence of any commercial or financial relationships that could be construed as a potential conflict of interest.

References

1. Vandenberghe S, Moskal P, Karp JS. State of the art in total body PET. EJNMMI Phys. 2020;7(1):3510.1186/s40658-020-00290-2.
2. Cherry SR, Jones T, Karp JS, Qi J, Moses WW, Badawi RD. Total-Body PET: Maximizing Sensitivity to Create New Opportunities for Clinical Research and Patient Care. J Nucl Med. 2018;59(1):3-1210.2967/jnumed.116.184028.
3. Tavare R, McCracken MN, Zettlitz KA, Salazar FB, Olafsen T, Witte ON, et al. Immuno-PET of Murine T Cell Reconstitution Postadoptive Stem Cell Transplantation Using Anti-CD4 and Anti-CD8 Cys-Diabodies. J Nucl Med. 2015;56(8):1258-6410.2967/jnumed.114.153338.
4. Pandit-Taskar N, Postow MA, Hellmann MD, Harding JJ, Barker CA, O'Donoghue JA, et al. First-in-Humans Imaging with (89)Zr-Df-IAB22M2C Anti-CD8 Minibody in Patients with Solid Malignancies: Preliminary Pharmacokinetics, Biodistribution, and Lesion Targeting. J Nucl Med. 2020;61(4):512-910.2967/jnumed.119.229781.
5. Yoon JK, Park BN, Ryu EK, An YS, Lee SJ. Current Perspectives on (89)Zr-PET Imaging. Int J Mol Sci. 2020;21(12)10.3390/ijms21124309.
6. Farwell MD, Gamache RF, Babazada H, Hellmann MD, Harding JJ, Korn R, et al. CD8-Targeted PET Imaging of Tumor-Infiltrating T Cells in Patients with Cancer: A Phase I First-in-Humans Study of (89)Zr-Df-IAB22M2C, a Radiolabeled Anti-CD8 Minibody. J Nucl Med. 2022;63(5):720-610.2967/jnumed.121.262485.
7. Man F, Khan AA, Carrascal-Minino A, Blower PJ, R TMdR. A kit formulation for the preparation of [(89)Zr]Zr(oxinate)4 for PET cell tracking: White blood cell labelling and comparison with [(111)In]In(oxinate)3. Nucl Med Biol. 2020;90-91:31-4010.1016/j.nucmedbio.2020.09.002.
8. Man F, Lim L, Volpe A, Gabizon A, Shmeeda H, Draper B, et al. In Vivo PET Tracking of (89)Zr-Labeled Vgamma9Vdelta2 T Cells to Mouse Xenograft Breast Tumors Activated with Liposomal Alendronate. Mol Ther. 2019;27(1):219-2910.1016/j.ymthe.2018.10.006.
9. Zhang J, He T, Xue L, Guo H. Senescent T cells: a potential biomarker and target for cancer therapy. EBioMedicine. 2021;68:10340910.1016/j.ebiom.2021.103409.
10. Falcke SE, Ruhle PF, Deloch L, Fietkau R, Frey B, Gaipl US. Clinically Relevant Radiation Exposure Differentially Impacts Forms of Cell Death in Human Cells of the Innate and Adaptive Immune System. Int J Mol Sci. 2018;19(11)10.3390/ijms19113574.
11. Weist MR, Starr R, Aguilar B, Chea J, Miles JK, Poku E, et al. PET of Adoptively Transferred Chimeric Antigen Receptor T Cells with (89)Zr-Oxine. J Nucl Med. 2018;59(10):1531-710.2967/jnumed.117.206714.
12. Nolz JC. Molecular mechanisms of CD8(+) T cell trafficking and localization. Cell Mol Life Sci. 2015;72(13):2461-7310.1007/s00018-015-1835-0.
13. Tantalo DG, Oliver AJ, von Scheidt B, Harrison AJ, Mueller SN, Kershaw MH, et al. Understanding T cell phenotype for the design of effective chimeric antigen receptor T cell therapies. J Immunother Cancer. 2021;9(5)10.1136/jitc-2021-002555.
14. Akbar AN, Henson SM. Are senescence and exhaustion intertwined or unrelated processes that compromise immunity? Nat Rev Immunol. 2011;11(4):289-9510.1038/nri2959.
15. Henson SM, Lanna A, Riddell NE, Franzese O, Macaulay R, Griffiths SJ, et al. p38 signaling inhibits mTORC1-independent autophagy in senescent human CD8(+) T cells. J Clin Invest. 2014;124(9):4004-1610.1172/JCI75051.
16. Kurebayashi Y, Choyke PL, Sato N. Imaging of cell-based therapy using (89)Zr-oxine ex vivo cell labeling for positron emission tomography. Nanotheranostics. 2021;5(1):27-3510.7150/ntno.51391.
17. Li M, Yao D, Zeng X, Kasakovski D, Zhang Y, Chen S, et al. Age related human T cell subset evolution and senescence. Immun Ageing. 2019;16:2410.1186/s12979-019-0165-8.
18. Hosokawa Y, Saga R, Monzen S, Terashima S, Tsuruga E. Ascorbic acid does not reduce the anticancer effect of radiotherapy. Biomed Rep. 2017;6(1):103-710.3892/br.2016.819.
19. Akbar AN, Henson SM, Lanna A. Senescence of T Lymphocytes: Implications for Enhancing Human Immunity. Trends Immunol. 2016;37(12):866-7610.1016/j.it.2016.09.002.

20. Callender LA, Carroll EC, Beal RWJ, Chambers ES, Nourshargh S, Akbar AN, et al. Human CD8(+) EMRA T cells display a senescence-associated secretory phenotype regulated by p38 MAPK. Aging Cell. 2018;17(1)10.1111/acel.12675.
21. Pulko V, Davies JS, Martinez C, Lanteri MC, Busch MP, Diamond MS, et al. Human memory T cells with a naive phenotype accumulate with aging and respond to persistent viruses. Nat Immunol. 2016;17(8):966-7510.1038/ni.3483.
22. Galgano A, Barinov A, Vasseur F, de Villartay JP, Rocha B. CD8 Memory Cells Develop Unique DNA Repair Mechanisms Favoring Productive Division. PLoS One. 2015;10(10):e014084910.1371/journal.pone.0140849.
23. d'Adda di Fagagna F, Reaper PM, Clay-Farrace L, Fiegler H, Carr P, Von Zglinicki T, et al. A DNA damage checkpoint response in telomere-initiated senescence. Nature. 2003;426(6963):194-810.1038/nature02118.
24. Chen WT, Ebelt ND, Stracker TH, Xhemalce B, Van Den Berg CL, Miller KM. ATM regulation of IL-8 links oxidative stress to cancer cell migration and invasion. Elife. 2015;410.7554/eLife.07270.
25. Guo H, Liu Z, Xu B, Hu H, Wei Z, Liu Q, et al. Chemokine receptor CXCR2 is transactivated by p53 and induces p38-mediated cellular senescence in response to DNA damage. Aging Cell. 2013;12(6):1110-2110.1111/acel.12138.
26. Lau EYM, Carroll EC, Callender LA, Hood GA, Berryman V, Pattrick M, et al. Type 2 diabetes is associated with the accumulation of senescent T cells. Clin Exp Immunol. 2019;197(2):205-1310.1111/cei.13344.
27. Muroyama Y, Manne S, Wellhausen N, Oldridge DA, Greenplate AR, Chilukuri L, et al. Induction of a CD8 T cell intrinsic DNA damge and repair response is associated with clinical reponse to PD-1 blockade in uterine cancer. https://doi.org/10.1101/2022.04.16.488552.

Figure legends

Figure 1. [^{89}Zr]Zr (oxinate)$_4$ chelation, ^{89}Zr cell labelling efficiency and ^{89}Zr retained during cell culture. A. Example of radio-TLC to determine [^{89}Zr]Zr-(oxinate)$_4$ chelation efficiency, with region of interest (ROI) region 1, (Rf = 0.139), being free ^{89}Zr, indicating 5.9% and ROI 2, (Rf = 0.869) being [^{89}Zr]Zr-(oxinate)$_4$, indicating 94.1%. **B.** Change in cell numbers in response to [^{89}Zr]Zr-(oxinate)$_4$ labelling, normalized to 1 × 10^6 cells. Young PBMC (n = 4) and Old PBMC (n = 3). **C.** [^{89}Zr]Zr-(oxinate)$_4$ cell labelling efficiency with young fresh PBMC (n = 3), young PBMC, Cryo (n = 5), old PBMC, Cryo, old (n = 3). **D.** % ^{89}Zr remaining associated with cells based on initial activity (%IA), and **E.** % ^{89}Zr remaining associated with cells comparing activity in cells and the cell culture supernatant at day one and four of cell culture of Young PBMC (n=3), Young PBMC Cryo (n=5), Old PBMC Cryo (n=3). Statistical analysis was determined using Mann Whitney U test, *** = $p < 0.005$.

Figure 2. The influence of ^{89}Zr on cell survival, CD8+ T cell Annexin V, and γH2AX expression. A. Enumeration of untreated Control PBMCs having seen no ^{89}Zr, Control Cryo, ^{89}Zr, ^{89}Zr Cryo, ^{89}Zr Cryo old, before labelling and at one- and four-days post labelling (n= 3 each, with two replicates). **B.** Number of CD8+ T cells per 10^6 PBMCs in culture after one and four days. **C.** Proportion (%) of Annexin V+ cells among control and ^{89}Zr labelled CD8+ T cells, at one and four days of culture (n = 3-5). **D.** Flow histograms showing γH2AX expression in CD8+ T cells among control and ^{89}Zr labelled young and old CD8+ T cells, before labelling, at one and four days of culture. **E.** Bar-graphs of γH2AX in CD8+ T cells following ^{89}Zr labelling and culture (n = 3, with two replicates). **F.** γH2AX positive CD8+ T cells per 10^6 PBMCs following ^{89}Zr labelling and culture (n = 3-5 with one or two replicates per experiment). Statistical analysis was performed using Mann Whitney U test, * = $p < 0.05$, *** = $p < 0.005$.

Figure 3. The phenotypic response of young and old CCR7/CD45RA defined CD8+ T cell subsets to ^{89}Zr labelling. A. Representative flow cytometry plots showing CD45RA/CCR7 defined CD8+ T cell subsets before labelling and among labelled young and old T cells at days one and four of cell culture. **B-E.** The proportions of CD8+ T cell subsets. **F-I.** Amount of CD8+ T cell subsets among control and ^{89}Zr labelled PBMCs or CD8+ T cells per 10^6 PBMCs at one and four days of culture (n = 3-6). Statistical analysis was performed using Mann Whitney U test, * = $p < 0.05$.

Figure 4. The DNA damage response of young and old CCR7/CD45RA defined CD8+ T cell subsets in response to ^{89}Zr labelling. A-D. Proportion of (A) Naïve γH2AX+, (B) CM γH2AX+, (C) EM γH2AX+ and (D) EMRA γH2AX+ T cells before labelling and among labelled cells and control cells at one and four days of cell culture. **E-H.** Amount of γH2AX+ CD8+ (E)

Naive, (F) CM, (G) EM and (H) EMRA T cells among control and ^{89}Zr labelled PBMCs per 10^6 PBMCs at one and four days of culture (n = 3-6). Statistical analysis was performed using Mann Whitney U test, * = p <0.05, ** = p < 0.01, *** = p < 0.005.

Figure 5. Strategies to prevent radiation induced CD8+ T cell cell-damage and expression of Annexin V and γH2AX. During the [^{89}Zr]Zr-(oxinate)$_4$ labelling reaction PBMCs underwent standard incubation (37°C), incubation at 4°C (4°C), incubation with 10 or 0.1 mg/mL ascorbic acid (10VitC, 0.1VitC) at 37°C or 50 µM 2-ME (2-ME) at 37°C. **A.** Labelling efficiency of PBMCs labelled with 50mBq/cell, [^{89}Zr]Zr-(oxinate)$_4$ with the above mentioned treatments. **B.** ^{89}Zr retained at one and four days of cell culture, conditions as described. **C.** Annexin V and **D.** γH2AX expression in CD8+ T cells at one and four days of cell culture subsequent to ^{89}Zr cell labelling with the above-mentioned treatment (n=3).

Figure 6. Tracking of ^{89}Zr labelled CD8+ T cell localization using preclinical PET/CT. NSG mice were infused with ^{89}Zr labelled 3 × 10^6 CD8+ T cells from a young (**A-C, G**) and an old individual (**D-F, H**), 36.9 ± 42.8 kBq/mouse. Mice were subjected to whole-body preclinical PET at 3 hr (2 hr scan, A, D), 24 hr (2 hr scan B, E) and 72 hr (3 hr scan, C, F). **G, H**. Transverse section (black arrowheads 3A and 3D) at time-points 3, 24 and 72hr highlighting regions with lungs, livers and spleens. White arrows indicate lung (lu), liver (li) and spleen (sp). Data was reconstructed and analysed using Vivoquant. **I – K.** Activities (%IA/g) in ROIs representing (G) Spleen, (H) Liver and (I) Lung at time points, 3hr, 24hr and 72hr. Shown is a representative experiment (n = 3).

Figure 1

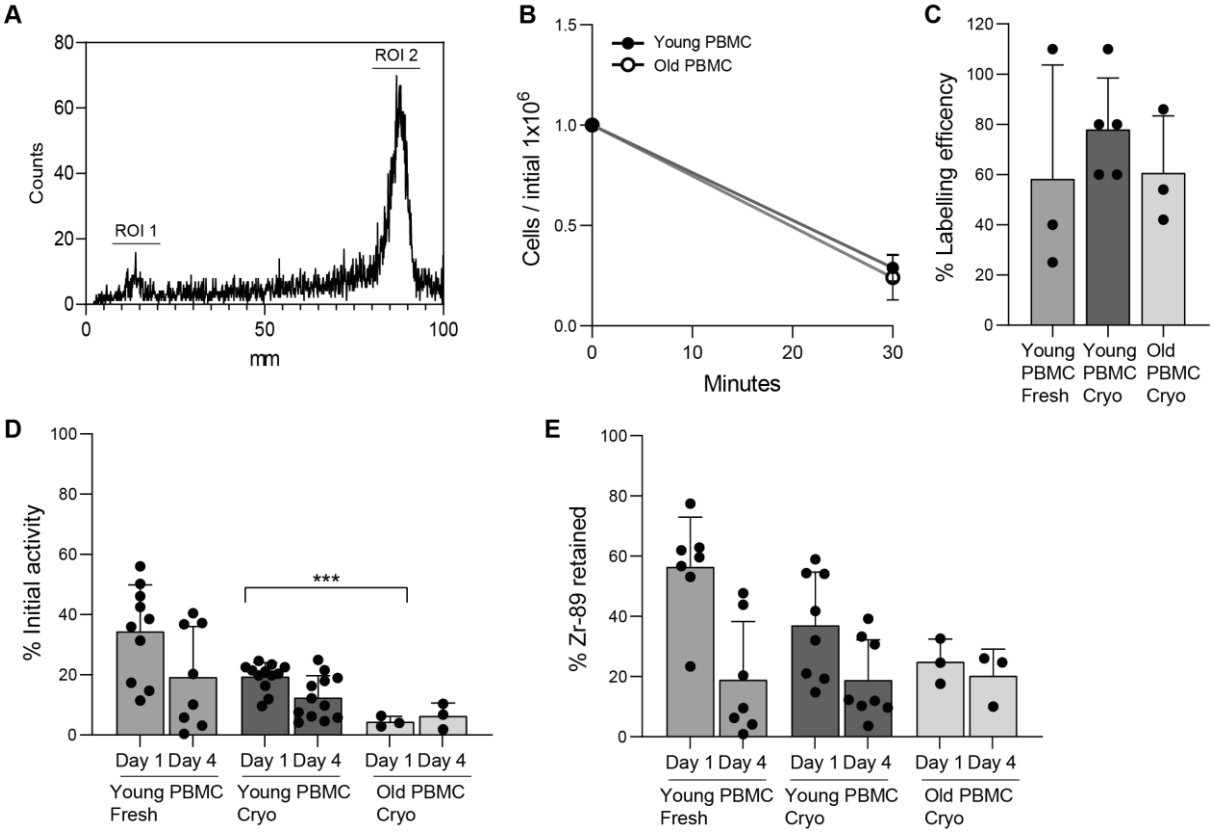
A
Counts
ROI 1
ROI 2
mm
B
Young PBMC
Old PBMC
Cells / intial 1x10^6
Minutes
C
% Labelling efficency
Young PBMC Fresh
Young PBMC Cryo
Old PBMC Cryo
D
% Initial activity
***
Day 1 Day 4
Young PBMC Fresh
Young PBMC Cryo
Old PBMC Cryo
E
% Zr-89 retained
Day 1 Day 4
Young PBMC Fresh
Young PBMC Cryo
Old PBMC Cryo

Figure 2

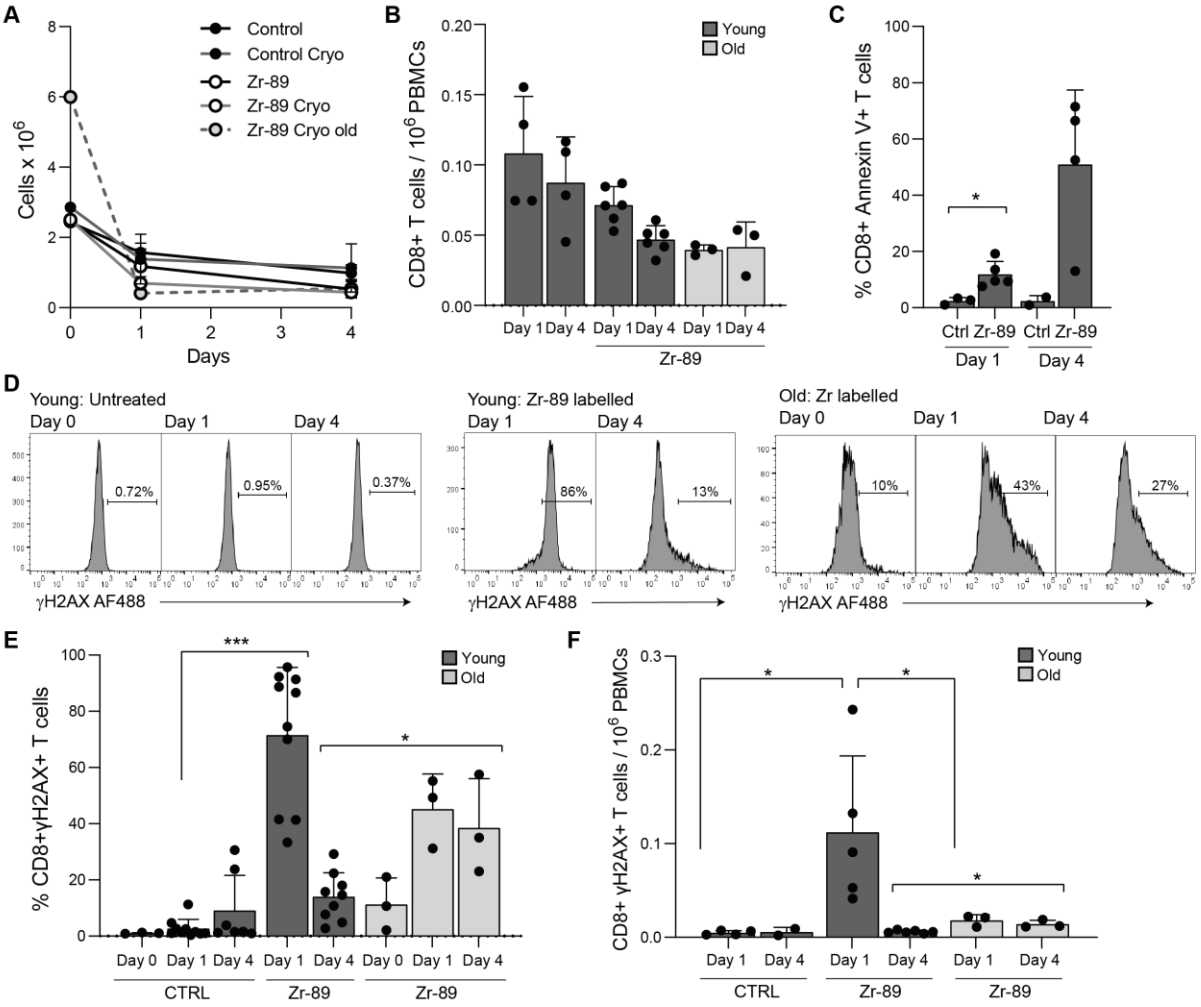
A
Control
Control Cryo
Zr-89
Zr-89 Cryo
Zr-89 Cryo old
Cells x 10^6
Days
B
Young
Old
CD8+ T cells / 10^6 PBMCs
Day 1 Day 4 Day 1 Day 4 Day 1 Day 4
Zr-89
C
% CD8+ Annexin V+ T cells
Ctrl Zr-89 Ctrl Zr-89
Day 1
Day 4
D
Young: Untreated
Day 0
Day 1
Day 4
0.72%
0.95%
0.37%
Young: Zr-89 labelled
Day 1
Day 4
86%
13%
Old: Zr labelled
Day 0
Day 1
Day 4
10%
43%
27%
γH2AX AF488
E
% CD8+γH2AX+ T cells
Young
Old
Day 0 Day 1 Day 4 Day 1 Day 4 Day 0 Day 1 Day 4
CTRL
Zr-89
Zr-89
F
CD8+ γH2AX+ T cells / 10^6 PBMCs
Day 1 Day 4 Day 1 Day 4 Day 1 Day 4
CTRL
Zr-89
Zr-89

Figure 3

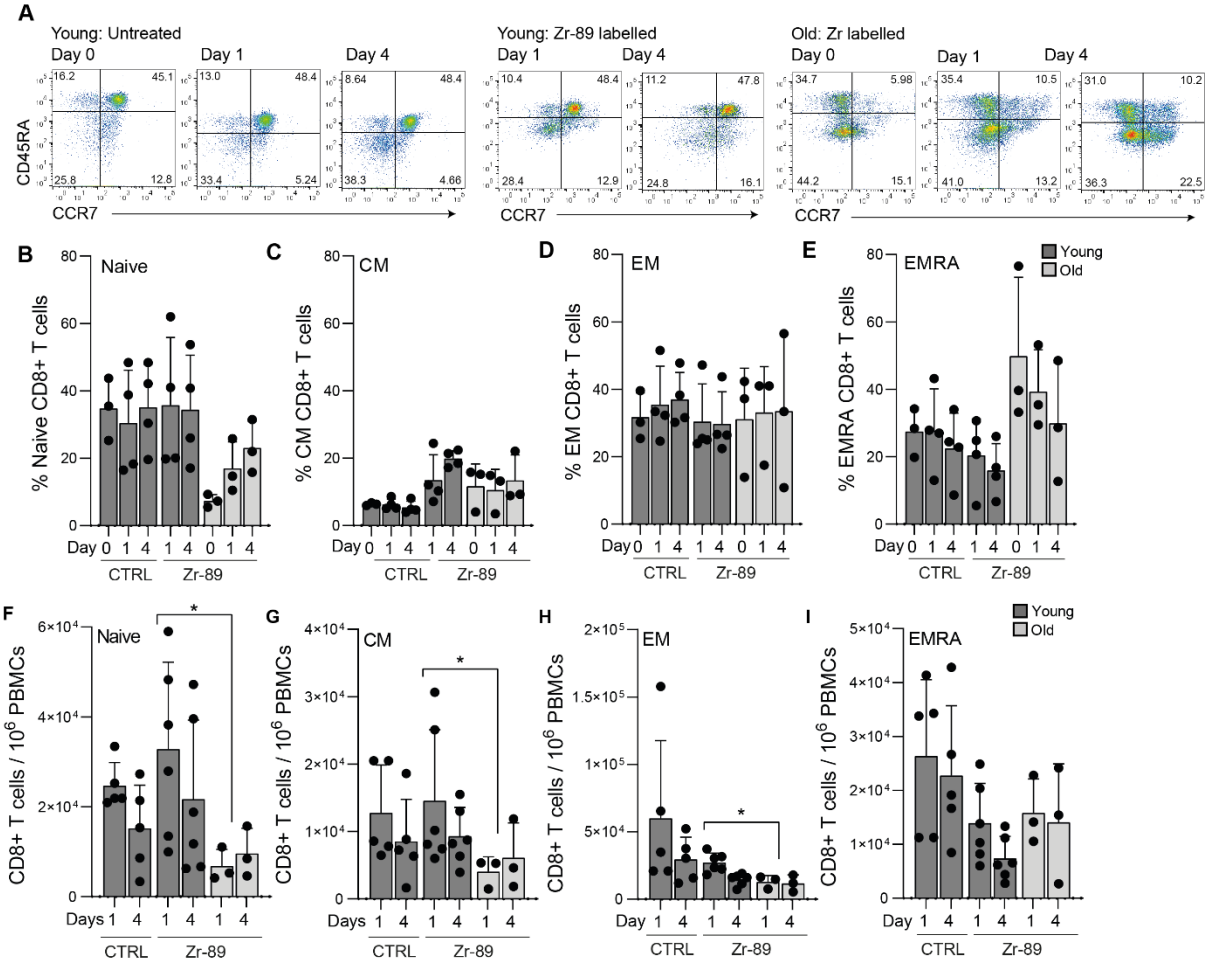
A
Young: Untreated
Day 0
Day 1
Day 4
Young: Zr-89 labelled
Day 1
Day 4
Old: Zr labelled
Day 0
Day 1
Day 4
CD45RA
CCR7
B
Naive
% Naive CD8+ T cells
C
CM
% CM CD8+ T cells
D
EM
% EM CD8+ T cells
E
EMRA
% EMRA CD8+ T cells
Young
Old
Day
CTRL
Zr-89
F
Naive
CD8+ T cells / 10^6 PBMCs
G
CM
H
EM
I
EMRA
Days

Figure 4

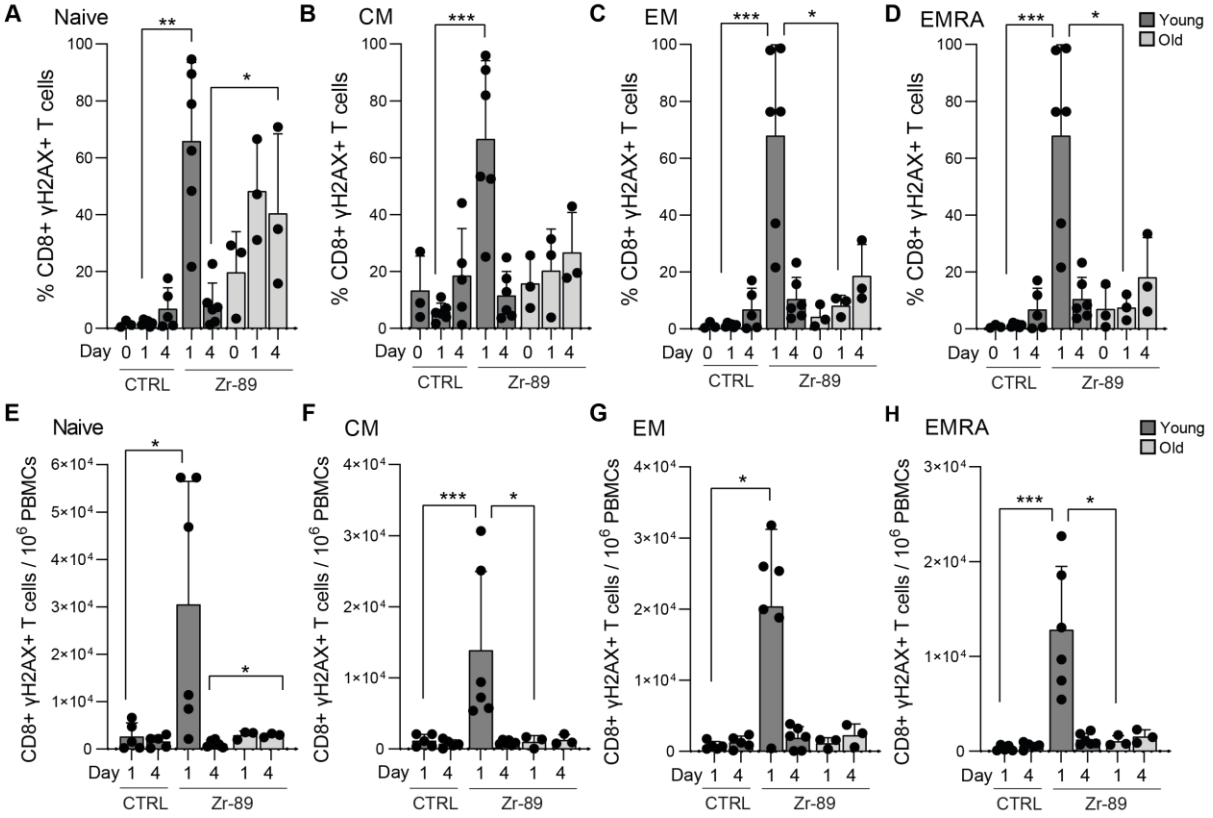
A
Naive
B
CM
C
EM
D
EMRA
Young
Old
% CD8+ γH2AX+ T cells
Day 0 1 4 1 4 0 1 4
CTRL
Zr-89
E
Naive
F
CM
G
EM
H
EMRA
CD8+ γH2AX+ T cells / 10^6 PBMCs
Day 1 4 1 4 1 4
CTRL
Zr-89

Figure 5

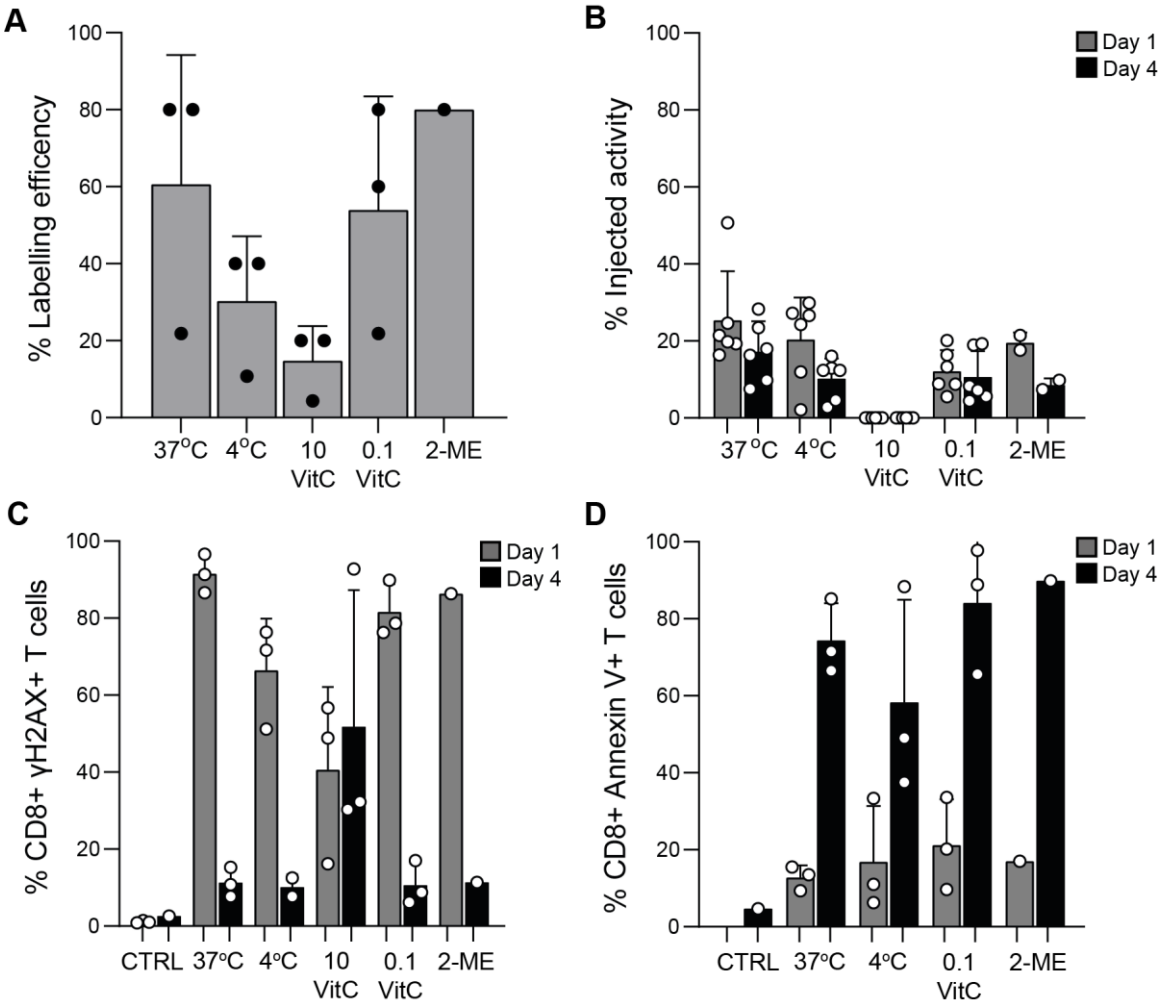
A
% Labelling efficency
100
80
60
40
20
0
37°C
4°C
10 VitC
0.1 VitC
2-ME
B
% Injected activity
Day 1
Day 4
C
% CD8+ γH2AX+ T cells
CTRL
D
% CD8+ Annexin V+ T cells

Figure 6

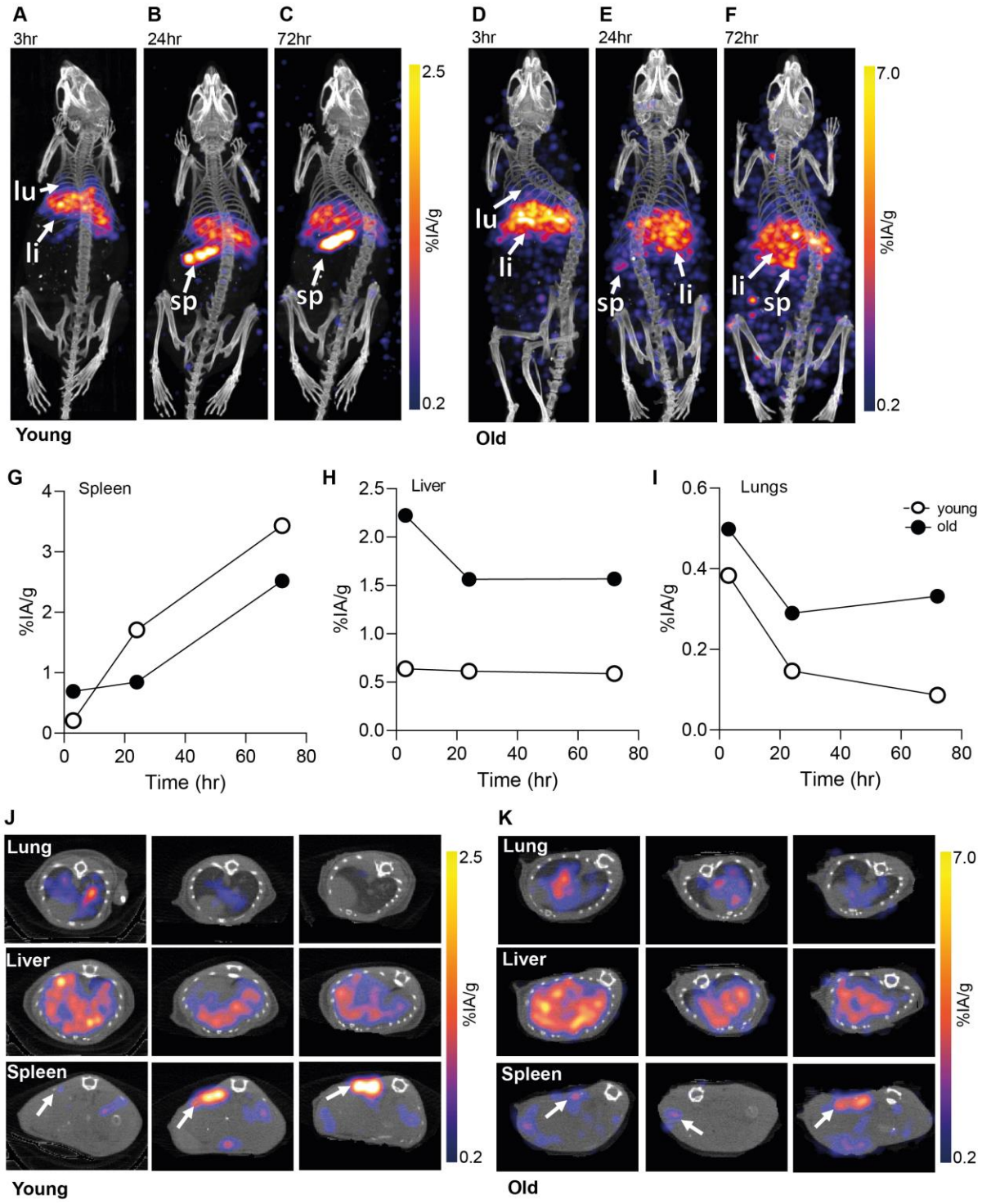
A
3hr
B
24hr
C
72hr
D
3hr
E
24hr
F
72hr
lu
li
sp
2.5
0.2
7.0
%IA/g
Young
Old
G
Spleen
H
Liver
I
Lungs
young
old
Time (hr)
J
K
Lung
Liver
Spleen